Journal of Solid State Chemistry 183 (2010) 180–185

Contents lists available at ScienceDirect

Journal of Solid State Chemistry

journal homepage: www.elsevier.com/locate/jssc

Neutron powder diffraction study of tetragonal $Li_7La_3Hf_2O_{12}$ with the garnet-related type structure

Junji Awaka [a,*,1], Norihito Kijima [a], Kunimitsu Kataoka [a,b], Hiroshi Hayakawa [a], Ken-ichi Ohshima [b], Junji Akimoto [a]

[a] National Institute of Advanced Industrial Science and Technology (AIST), Tsukuba Central 5, 1-1-1 Higashi, Tsukuba, Ibaraki 305-8565, Japan
[b] Graduate School of Pure and Applied Sciences, University of Tsukuba, 1-1-1 Tennodai, Tsukuba, Ibaraki 305-8573, Japan

ARTICLE INFO

Article history:
Received 10 September 2009
Received in revised form
26 October 2009
Accepted 29 October 2009
Available online 10 November 2009

Keywords:
Garnet
Neutron powder diffraction
X-ray powder diffraction
Rietveld analysis
Lithium-ion conductor

ABSTRACT

We have successfully synthesized a polycrystalline sample of tetragonal garnet-related Li-ion conductor $Li_7La_3Hf_2O_{12}$ by solid state reaction. The crystal structure is analyzed by the Rietveld method using neutron powder diffraction data. The structure analysis identifies that tetragonal $Li_7La_3Hf_2O_{12}$ has the garnet-related type structure with a space group of $I4_1/acd$ (no. 142). The lattice constants are $a=13.106(2)$ Å and $c=12.630(2)$ Å with a cell ratio of $c/a=0.9637$. The crystal structure of tetragonal $Li_7La_3Hf_2O_{12}$ has the garnet-type framework structure composed of dodecahedral $La(1)O_8$, $La(2)O_8$ and octahedral HfO_6. Li atoms occupy three types of crystallographic site in the interstices of this framework structure, where Li(1) atom is located at the tetrahedral 8*a* site, and Li(2) and Li(3) atoms are located at the distorted octahedral 16*f* and 32*g* sites, respectively. These Li sites are filled with the Li atom. The present tetragonal $Li_7La_3Hf_2O_{12}$ sample exhibits bulk Li-ion conductivity of $\sigma_b=9.85\times10^{-7}$ S cm^{-1} and grain-boundary Li-ion conductivity of $\sigma_{gb}=4.45\times10^{-7}$ S cm^{-1} at 300 K. The activation energy is estimated to be $E_a=0.53$ eV in the temperature range of 300–580 K.

1. Introduction

Lithium-ion conductors with the garnet-related type structure have gained considerable attention as the electrolyte of the all-solid-state rechargeable Li-ion batteries. Especially, garnet-related $Li_7La_3Zr_2O_{12}$ exhibits the high bulk conductivity σ_b around 10^{-4} S cm^{-1} at room temperature ($E_a\approx0.3$ eV at 291–573 K), and has good thermal stability and chemical stability against molten lithium, air, and moisture [1,2].

The garnet-related Li-ion conductors belonged to cubic and tetragonal symmetries were reported. $Li_5La_3A_2O_{12}$ (A=Nb, Ta, Sb, Bi) and $Li_7La_3Zr_2O_{12}$ show the cubic symmetry [1–18], and $Li_7La_3Zr_2O_{12}$ and $Li_7La_3Sn_2O_{12}$ show the tetragonal symmetry [19,20]. The crystal structure of cubic garnet-related Li-ion conductors, for example, Ta-containing compounds, has the garnet-type framework structure composed of dodecahedral LaO_8 and octahedral TaO_6. Li atoms occupy the tetrahedral site and the distorted octahedral site with split-atom model in the interstices of this framework structure, and show the occupational disordering in these sites. In the ideal garnet-type structure [21–27], for instance, $Y_3Al_5O_{12}$ and $Y_3Fe_5O_{12}$, the tetrahedral site is fully occupied by the metal cation, and the distorted octahedron is vacant. This complicated Li arrangement, as shown in Refs. [14–18], is the significant characteristic of the cubic garnet-related Li-ion conductors. On the other hand, $Li_7La_3Zr_2O_{12}$ and $Li_7La_3Sn_2O_{12}$ were recently reported to have tetragonal symmetry with a space group of $I4_1/acd$ (no. 142) [19,20]. The framework structure of these compounds is garnet-type structure similar to the cubic garnet-related Li-ion conductors. Li atoms are also located in same coordination with the tetrahedron and the distorted octahedron. However, these polyhedra are completely ordered by both Li atom and vacancy. The Li arrangement is an important distinction between the cubic and tetragonal garnet-related Li-ion conductors.

The two stable phases with cubic and tetragonal symmetries were reported in $Li_7La_3Zr_2O_{12}$ [1,2,19], which depends on the synthesis temperature. Tetragonal $Li_7La_3Zr_2O_{12}$ was prepared by heating at a lower temperature than synthesis temperature of cubic $Li_7La_3Zr_2O_{12}$. In this work, tetragonal $Li_7La_3Hf_2O_{12}$ was successfully synthesized by adapted the same temperature program sequences of tetragonal $Li_7La_3Zr_2O_{12}$. Tetragonal $Li_7La_3Hf_2O_{12}$ is a new member of the fast Li-ion conductor having garnet-related type structure. The crystal structure of this compound was investigated by the Rietveld method using neutron powder diffraction (ND) data. The results of the structure analysis and ac impedance measurements were compared to those of tetragonal $Li_7La_3Zr_2O_{12}$.

* Corresponding author.
E-mail address: j.awaka@aist.go.jp (J. Awaka).
[1] Research Fellow of the Japan Society for the Promotion of Science.

0022-4596/$ - see front matter © 2009 Elsevier Inc. All rights reserved.
doi:10.1016/j.jssc.2009.10.030

2. Experimental

Polycrystalline tetragonal $Li_7La_3Hf_2O_{12}$ was prepared by the solid-state reaction:

$$7Li_2CO_3 + 3La_2O_3 + 4HfO_2 \rightarrow 2Li_7La_3Hf_2O_{12} + 7CO_2\uparrow. \quad (1)$$

The starting materials (purity: 99.9%) of Li_2CO_3, La_2O_3 (pre-dried at 1173 K for 12 h), and HfO_2 were mixed in the calculated ratio, where 10 wt% excess Li_2CO_3 was added to compensate the loss of the lithium component by volatilization at high temperature. Mixed powder materials were put in an alumina crucible and heated at 1173 K for 5 h in ambient atmosphere. The calcined specimen was reground and heated at 1253 K for 5 h.

Chemical analysis of the Li, La, and Hf content of the products was carried out using inductively coupled plasma-optical emission spectroscopy (ICP-OES) using an Optima 3000 (Perkin Elmer).

The ND data were collected at room temperature using a Kinken powder diffractometer for high efficiency and high resolution measurements, HERMES, at the Institute for Materials Research (IMR), Tohoku University, installed at the JRR-3M reactor of the Japan Atomic Energy Agency (JAEA), Tokai [28]. Neutrons with a wavelength of 1.8204(5) Å were obtained by the 331 reflection of the Ge monochromator and 12′-blank-sample-22′ collimation. Diffraction data were collected at step intervals of 0.1° over a 2θ range from 7° to 157°.

X-ray powder diffraction (XRD) data were collected at room temperature using a Rigaku RINT2550V diffractometer equipped with a curved graphite monochromator. The open angle of the divergence and scattering slits were both 0.5°, and the width of the receiving slit was 0.15 mm. The X-ray (Cu$K\alpha$ radiation) tube voltage and tube electric current were 30 kV and 100 mA, respectively. Diffraction data were collected at step intervals of 0.02° over a 2θ range from 5° to 120°. The fixed counting time in the XRD measurements was 2 s.

The XRD and ND data were analyzed by the Rietveld method with a computer program RIETAN-2000 [29]. The split pseudo-Voigt profile function was used as the profile function in the refinement. A partial profile relaxation with a modified split pseudo-Voigt function was applied to some reflections [29]. The crystal structure was drawn using a computer program VESTA [30].

AC impedance measurements were conducted using a Solartron 1260 impedance analyzer operating at 100 mV applied ac amplitude, at 13 MHz–100 mHz frequencies, over the temperature range of 300–580 K in heating process, in air. The powder sample was pressed into a pellet at 0.2 GPa at room temperature. The pellet was covered with a powder of the same composition, and then sintered at 1273 K for 4 h. The sintered pellet was ground to a thin pellet using a diamond file. The obtained pellet was 12.11 mm in diameter and 1.00 mm thick, and the relative density of the sintered sample was 60%. The electrode connections were 8 mm in diameter, and were made from Au paste heated at 923 K for 10 min.

3. Results and discussion

3.1. Chemical analysis

Polycrystalline specimen of tetragonal $Li_7La_3Hf_2O_{12}$ was successfully synthesized through the solid state reaction. The melting point of starting materials is 891 K for Li_2CO_3, 2273 K for La_2O_3, and 3085 K for HfO_2. The low melting point and dissociation of Li_2CO_3 could presumably promote the homogeneity of the specimen in the chemical reaction stage [14].

The fine-powder specimen of tetragonal $Li_7La_3Hf_2O_{12}$ was white in color. Its chemical composition was determined to be Li:La:Hf=7.0:3.1:2.0 in atomic ratio by ICP-OES. The estimated value of oxygen content from the experimental value of Li (4.7 wt%), La (41 wt%), and Hf (35 wt%) was in good agreement with the calculated value for chemical composition of $Li_7La_3Hf_2O_{12}$ within the experimental error. From the compensation of electric charge, oxygen content was also calculated to be about 12 for Li:La:Hf=7.0:3.1:2.0. The chemical composition was analytically determined as $Li_7La_3Hf_2O_{12}$.

A small amount of Li_2CO_3 impurity was detected in the ND data of tetragonal $Li_7La_3Hf_2O_{12}$ prepared with the large amount of 15 g, as shown in Fig. 1. This Li_2CO_3 impurity arose from the additional Li_2CO_3 used in sample preparation. From the quantitative analysis of the multiphase specimen by later Rietveld analysis, mass fractions contained in the powder specimen were estimated 0.009 for Li_2CO_3 and 0.991 for tetragonal $Li_7La_3Hf_2O_{12}$.

3.2. Structure refinement

The crystal structure of tetragonal $Li_7La_3Hf_2O_{12}$ was analyzed by the Rietveld method using ND data. The structure model of tetragonal $Li_7La_3Zr_2O_{12}$ [19] was adapted as the initial structure

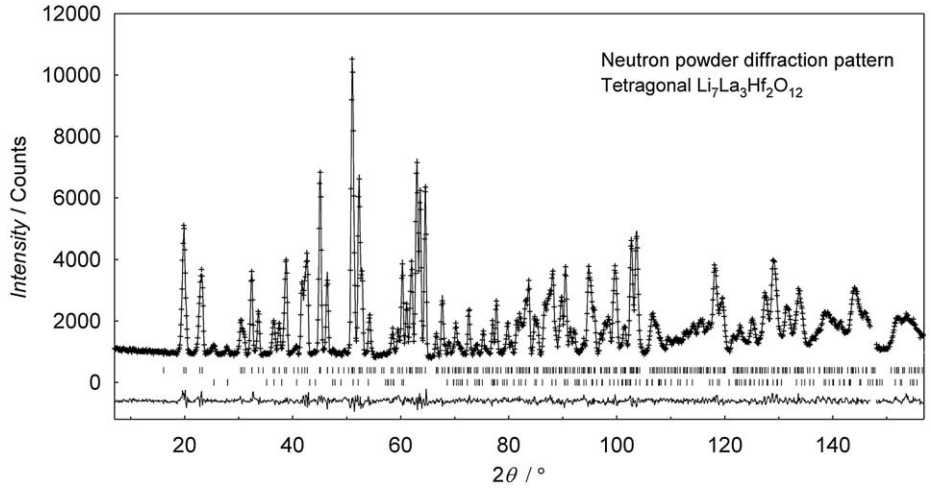

Fig. 1. Observed (+), calculated (solid line), and difference (bottom) patterns for the Rietveld refinement using the neutron powder diffraction data of tetragonal $Li_7La_3Hf_2O_{12}$. The short vertical lines below the profiles mark the peak positions of all possible Bragg reflections of tetragonal $Li_7La_3Hf_2O_{12}$ (upper) and Li_2CO_3 (lower).

Table 1
Crystallographic data and details of the structure refinements and data collection.

Chemical formula	$Li_7La_3Hf_2O_{12}$	
Radiation	Neutron	Cu$K\alpha$
Crystal system	Tetragonal	Tetragonal
Space group	$I4_1/acd$ (no. 142)	$I4_1/acd$ (no. 142)
Z	8	8
Lattice constant a (Å)	13.106(2)	13.107(2)
Lattice constant c (Å)	12.630(2)	12.637(2)
Cell ratio c/a	0.9637	0.9641
V (Å^3)	2169.3(5)	2170.8(4)
D_x (g cm^{-3})	6.211	6.207
Formula weight	1014.3	1014.3
R_{wp} (%)	3.81	14.68
R_e (%)	2.33	8.95
R_p (%)	2.97	10.91
R_B (%)	0.68	4.70
R_F (%)	0.31	3.03
S	1.63	1.64
Number of relaxed reflections	4	5
Wavelength (Å)	1.8204(5)	1.5418
2θ range (deg)	7.0–157	5.0–120
2θ step width (deg)	0.10	0.02

The R-values and S are defined in Ref. [34]. Numbers in parentheses are the estimated standard deviations of the last significant digit.

Table 2
Structure parameters of tetragonal $Li_7La_3Hf_2O_{12}$ determined from the neutron powder diffraction analysis.

Atom	Site	g	x	y	z	U (Å^2)
La(1)	8b	1	0	1/4	1/8	0.0022(8)
La(2)	16e	1	0.1270(2)	0	1/4	0.0027(6)
Hf	16c	1	0	0	0	0.0016(6)
Li(1)	8a	1	0	1/4	3/8	0.007(3)
Li(2)	16f	1	0.1773(7)	0.4273[(a)]	1/8	0.022(3)
Li(3)	32g	1	0.0802(5)	0.0856(6)	0.8045(5)	0.015(2)
O(1)	32g	1	−0.0331(2)	0.0546(2)	0.1520(2)	0.0037(7)
O(2)	32g	1	0.0537(2)	0.8536(2)	0.5340(2)	0.0048(7)
O(3)	32g	1	0.1486(2)	0.0271(2)	0.4471(2)	0.0037(6)

Definitions: g, occupation factor; x, y, and z, fractional coordinate. U is the isotropic atomic displacement parameter when the Debye–Waller factor is represented as $\exp(-8\pi^2 U \sin^2\theta/\lambda^2)$.
Linear constraints: (a) $y(\mathrm{Li}(2)) = 0.25 + x(\mathrm{Li}(2))$.

model. The Rietveld refinement was conducted by the tetragonal garnet-related structure with space group of $I4_1/acd$ (no. 142). The La(1), La(2), Hf, Li(1), and Li(2) sites were the special positions of 8b (the multiplicity and the Wyckoff letter), 16e, 16c, 8a, and 16f sites, respectively. The Li(3), O(1), O(2), and O(3) sites were the general positions of 32g site. The lattice constants of a and c used as the starting value were determined by the Cohen's method [31–33] using the XRD data. A small amount of Li_2CO_3 impurity was detected in the ND data, therefore the two-phase analysis involving Li_2CO_3 phase was conducted. The 2θ range from 147° to 148° was excluded because of the existence of the experimental error.

Fig. 1 shows observed, calculated, and difference patterns for Rietveld refinement of tetragonal $Li_7La_3Hf_2O_{12}$. All the diffraction peaks in the ND pattern were indexed on the basis of tetragonal symmetry with $I4_1/acd$, except for peaks from Li_2CO_3 impurity. Table 1 lists the crystallographic data and details of the structure refinements. The resultant R-values reached R_{wp}=3.81%, R_p=2.97%, R_B=0.68%, and R_F=0.31%, with a fit indicator of $S=R_{wp}/R_e$=1.63. Good agreement between the observed and calculated ND patterns has been shown in Fig. 1. The lattice constants were refined to be a=13.106(2) Å and c=12.630(2) Å. These values were slightly smaller than tetragonal $Li_7La_3Zr_2O_{12}$ with a=13.134(4) Å and c=12.663(8) Å. The cell ratio was c/a=0.9637, which is corresponding to 0.9641 of tetragonal $Li_7La_3Zr_2O_{12}$. Table 2 presents the structure parameters of tetragonal $Li_7La_3Hf_2O_{12}$. The final structure model of tetragonal $Li_7La_3Hf_2O_{12}$ was well-consistent with the tetragonal $Li_7La_3Zr_2O_{12}$.

Fig. 2 shows the XRD pattern of tetragonal $Li_7La_3Hf_2O_{12}$. The splitting of the diffraction lines, caused by a slight distortion of the tetragonal symmetry, was observed. For example, the splitting corresponding to 400 and 004 was clearly observed in the diffraction data around 2θ=27.2° and 28.2°, respectively. In the structure analysis using XRD data, the fractional coordinate of all atoms was fixed at the result of the ND analysis, and the atomic displacement parameter of all atoms was fixed at the value of tetragonal $Li_7La_3Zr_2O_{12}$ determined the single-crystal X-ray diffraction analysis reported in Ref. [19]. The final R-values were R_{wp}=14.68%, R_p=10.91%, R_B=4.70%, and R_F=3.03%, with S=1.64. The XRD pattern was identified as the single phase of tetragonal $Li_7La_3Hf_2O_{12}$ structure. The lattice constants were a=13.107(2) Å and c=12.637(2) Å, which was in good agreement with the results from the ND analysis.

Fig. 3 illustrates the crystal structure of tetragonal $Li_7La_3Hf_2O_{12}$. The cell ratio was $c/a \approx 0.964$, as presented in Table 1. The crystal structure was only distorted from the cubic

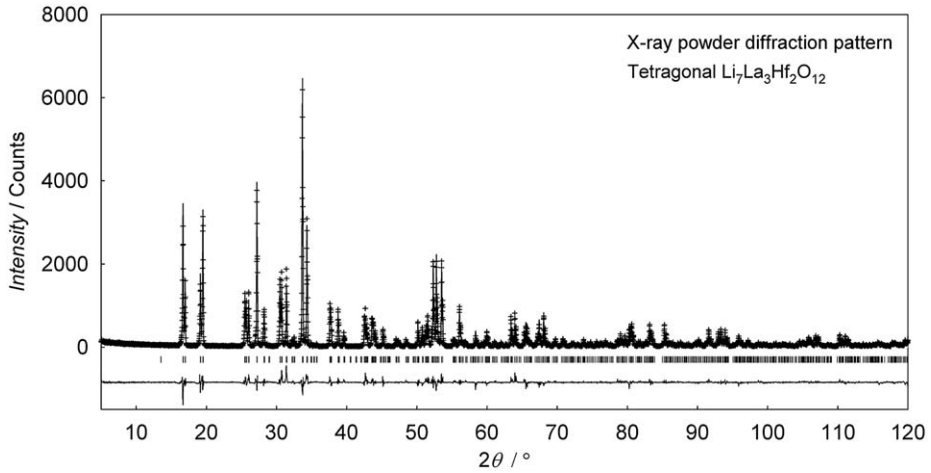

Fig. 2. Observed, calculated, and difference patterns for the Rietveld refinement using the X-ray powder diffraction data of tetragonal $Li_7La_3Hf_2O_{12}$. The short vertical lines below the profiles mark the peak positions of all possible Bragg reflections of tetragonal $Li_7La_3Hf_2O_{12}$.

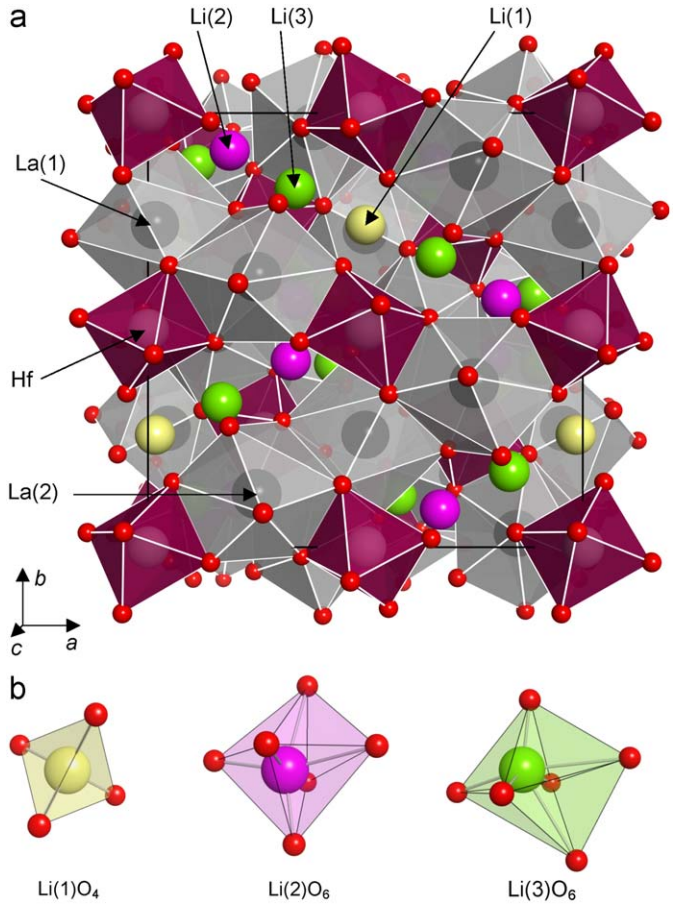

Fig. 3. (a) Crystal structure of tetragonal $Li_7La_3Hf_2O_{12}$. The solid box indicates the unit cell. (b) The coordination polyhedra of Li(1), Li(2), and Li(3) atoms.

lattice, leaving the garnet-related structure unchanged. The crystal structure of tetragonal $Li_7La_3Hf_2O_{12}$ had the garnet-type framework structure composed of dodecahedral $La(1)O_8$, $La(2)O_8$ and octahedral HfO_6. Table 3 presents the selected interatomic distances calculated from the crystal data obtained from ND data. The mean distance of La(1)–O and La(2)–O was 2.572 Å and 2.540 Å, respectively. These values were consistent with 2.588 Å for mean La(1)–O and 2.544 Å for mean La(2)–O of tetragonal $Li_7La_3Zr_2O_{12}$. The mean Hf–O was 2.090 Å, which was slightly shorter than the mean Zr–O=2.113 Å of tetragonal $Li_7La_3Zr_2O_{12}$. Here, the value of Hf^{4+}–O^{2-}=2.11 Å and Zr^{4+}–O^{2-}=2.12 Å with coordination number of 6 was calculated from the sum of shannon's ionic radii [35].

Li atoms occupied three types of crystallographic site in the interstices of the garnet-type framework structure, as shown in Fig. 3(a). These Li sites were filled with the Li atom. The Li–Li distance was 2.557(7) Å for Li(1)–Li(3), 2.592(10) Å and 2.605(7) Å for Li(2)–Li(3), and 2.632(10) Å for Li(3)–Li(3). Fig. 3(b) illustrates the coordination polyhedra of each Li atom. Li(1) atom occupied the tetrahedral 8*a* site; here the tetrahedral 16*e* site, which is the equivalent position to the tetrahedral 8*a* site in the cubic garnet-related structure, was completely vacant. Li(2) and Li(3) atoms occupied the distorted octahedral 16*f* and 32*g* sites, respectively. These distorted octahedra had two long Li–O bonds of 2.528(9) Å ($\times 2$) for $Li(2)O_6$ and 2.824(7) Å and 2.886(8) Å for $Li(3)O_6$. The mean distance of Li(1)–O, Li(2)–O, and Li(3)–O was 1.913 Å, 2.273 Å, and 2.315 Å, respectively, which were well-consistent with the reported value of tetragonal $Li_7La_3Zr_2O_{12}$.

The ideal garnet-type compounds are known to be generally cubic symmetry with *Ia*-3*d* (no. 230) [21–27]. However, non-cubic

Table 3
Selected interatomic distances of tetragonal $Li_7La_3Hf_2O_{12}$ determined from the neutron powder diffraction analysis.

Polyhedron	Bond	Count	Interatomic distance (Å)
$La(1)O_8$	La(1)–O(1)	×4	2.620(2)
	La(1)–O(2)[a]	×4	2.524(2)
$La(2)O_8$	La(2)–O(1)	×2	2.539(2)
	La(2)–O(2)[b]	×2	2.626(2)
	La(2)–O(3)[c]	×2	2.466(3)
	La(2)–O(3)	×2	2.531(2)
HfO_6	Hf–O(1)	×2	2.094(2)
	Hf–O(2)[a]	×2	2.088(2)
	Hf–O(3)[d]	×2	2.089(2)
$Li(1)O_4$	Li(1)–O(2)[e]	×4	1.913(2)
$Li(2)O_6$	Li(2)–O(1)[f]	×2	1.936(9)
	Li(2)–O(3)[g]	×2	2.355(3)
	Li(2)–O(3)[h]	×2	2.528(9)
$Li(3)O_6$	Li(3)–O(1)[i]	×1	2.015(8)
	Li(3)–O(1)[j]	×1	2.063(7)
	Li(3)–O(2)[k]	×1	2.217(7)
	Li(3)–O(2)[l]	×1	2.824(7)
	Li(3)–O(2)[m]	×1	2.886(8)
	Li(3)–O(3)[n]	×1	1.882(7)

Symmetry codes: (a) x, $1-y$, $1/2-z$; (b) $-3/4+y$, $-1/4+x$, $3/4-z$; (c) $1/4+y$, $1/4-x$, $-1/4+z$; (d) x, $-y$, $1/2-z$; (e) $-x$, $1-y$, $1-z$; (f) $-x$, $1/2-y$, z; (g) $1/4-y$, $1/4+x$, $3/4-z$; (h) $1/4-y$, $3/4-x$, $-1/4+z$; (i) $-x$, $-y$, $1-z$; (j) $-x$, y, $1/2+z$; (k) x, $1-y$, $3/2-z$; (l) $3/4-y$, $1/4-x$, $1/4+z$; (m) $-3/4+y$, $1/4+x$, $1/4+z$; (n) $1/4-y$, $1/4-x$, $5/4-z$.

garnets were reported, for example, the majorite garnet of $\{Mg_3\}[MgSi](Si_3)O_{12}$ and $\{Mn_3\}[MnSi](Si_3)O_{12}$ have the tetragonal symmetry according to $I4_1/a$ (no. 88) [36–39]. These tetragonal garnets exhibit the Mg (or Mn) and Si ordering on two symmetrically distinct octahedral sites. $\{Mg_3\}[MgSi](Si_3)O_{12}$ was also reported that the crystal structure was cubic symmetry with complete Mg–Si disordering on the octahedral site in the transition zone at high temperature and pressure [39]. For these ideal garnets, the origin of the phase transition from cubic to lower symmetry of tetragonal is interpreted by the cation ordering. The cubic garnet-related Li-ion conductors have the complicated Li arrangement with the occupational disordering in tetrahedral and distorted octahedral sites [14–18]. On the other hand, the tetragonal garnet-related Li-ion conductors were characterized by the fully ordered Li arrangement on these sites. The Li arrangement is an important distinction between the cubic and tetragonal garnet-related Li-ion conductors. In the garnet-related structure, the ordered Li arrangement may be the origin of the tetragonal symmetry.

3.3. Ionic conductivity

Fig. 4 shows a Nyquist plot of the ac impedance spectra for the sintered sample of tetragonal $Li_7La_3Hf_2O_{12}$. The steep rise of the impedance plot in the low-frequency range is typically expected for the blocking of mobile Li ions at the electrode interface, which is evidence that tetragonal $Li_7La_3Hf_2O_{12}$ is a Li-ion conductor. The impedance plot in the high-frequency range displayed two-semicircle behavior. Tetragonal $Li_7La_3Zr_2O_{12}$ has similar features [19]. The resistance component on the high frequency side was the bulk contribution, and the other was the grain-boundary contribution. Each semicircle was interpreted as an equivalent circuit consisting of a parallel combination of a resistance and a capacitance. Therefore, the overall behavior of the impedance plot can be fitted by an equivalent circuit of $(R_bQ_b)(R_{gb}Q_{gb})(Q_{el})$, where R is the resistance, Q the constant phase element for the capacitive

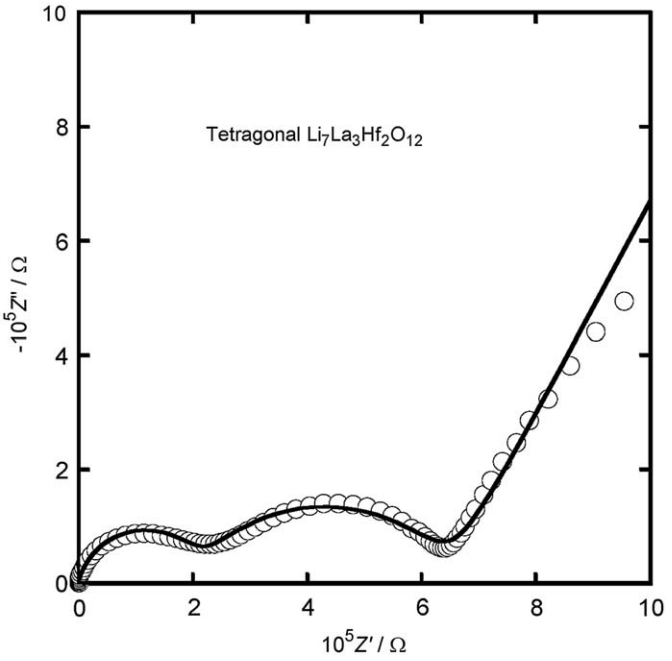

Fig. 4. Nyquist plot of the ac impedance spectra for the sintered sample of tetragonal $Li_7La_3Hf_2O_{12}$ with Li-blocking Au electrodes at 300 K in air. The open circles show experimental results, and the solid curve shows the calculated result with an equivalent circuit of $(R_bQ_b)(R_{gb}Q_{gb})(Q_{el})$.

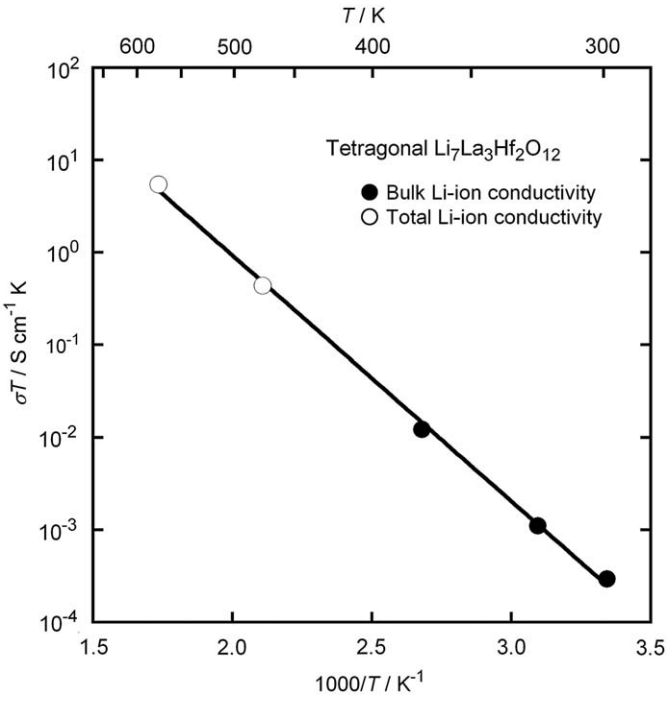

Fig. 5. Temperature dependence of the Li-ion conductivity of tetragonal $Li_7La_3Hf_2O_{12}$. The solid and open circles show bulk Li-ion conductivity and total (sum of the bulk and grain-boundary contributions) Li-ion conductivity, respectively.

element, and the subscripts b, gb, and el with each notation represent the bulk, grain-boundary, and electrode, respectively. The conductivities were obtained by analyzing the impedance plots using a computer program ZView3.0. The bulk conductivity was $\sigma_b = 9.85 \times 10^{-7}$ S cm^{-1}, and the grain-boundary conductivity was $\sigma_{gb} = 4.45 \times 10^{-7}$ S cm^{-1} at 300 K ($\sigma_b = 3.44 \times 10^{-6}$ S cm^{-1} and $\sigma_{gb} = 3.06 \times 10^{-6}$ S cm^{-1} at 320 K).

Cubic garnet-related Li-ion conductors were reported that their Li-ion conductivity was depended on the lattice size [8,9], for example, $Li_6CaLa_2Ta_2O_{12}$ with lattice constant of $a = 12.725(2)$ Å was the total (sum of bulk and grain-boundary contributions) conductivity of $\sigma_{total} = 2.2 \times 10^{-6}$ S cm^{-1}, $Li_6SrLa_2Ta_2O_{12}$ with $a = 12.808(2)$ Å was $\sigma_{total} = 7.0 \times 10^{-6}$ S cm^{-1}, and $Li_6BaLa_2Ta_2O_{12}$ with $a = 13.001(4)$ Å was $\sigma_{total} = 1.3 \times 10^{-5}$ S cm^{-1} around room temperature [8,9,14]. Tetragonal $Li_7La_3Zr_2O_{12}$ exhibited the bulk conductivity of $\sigma_b = 1.63 \times 10^{-6}$ S cm^{-1} at 300 K [19]. The Li-ion conductivity of tetragonal $Li_7La_3Hf_2O_{12}$ with $a = 13.106(2)$ Å and $c = 12.630(2)$ Å was slightly lower than that of tetragonal $Li_7La_3Zr_2O_{12}$ with $a = 13.134(4)$ Å and $c = 12.663(8)$ Å. The Li-ion conductivity of tetragonal garnet-related Li-ion conductors was also depended on the lattice size.

Fig. 5 shows the Li-ion conductivity as a function of $1/T$ for a sintered sample of tetragonal $Li_7La_3Hf_2O_{12}$. The conductivity could not be separated into bulk and grain-boundary contributions above 370 K, therefore the total conductivity was plotted above 370 K in Fig. 5. The temperature dependence of the conductivity can be expressed by the Arrhenius equation,

$$\sigma = \frac{A}{T} \exp\left(\frac{-E_a}{k_B T}\right), \tag{2}$$

where A is the pre-exponential factor, T the absolute temperature, E_a the activation energy, and K_B the Boltzmann constant. The activation energy was estimated to be $E_a = 0.53$ eV from the slope of the $\log \sigma T$ versus $1/T$ plot in the temperature range of 300–580 K, and was in good agreement with that of tetragonal $Li_7La_3Zr_2O_{12}$ ($E_a = 0.54$ eV at 300–560 K).

Tetragonal garnet-related Li-ion conductors showed a lower Li-ion conductivity than the cubic garnet-related Li-ion conductors. The suppressed hopping between Li sites by the complete Li ordering, and by the decrease in equivalent Li positions compared to the cubic garnet-related Li-ion conductors may result in the low Li-ion conduction of tetragonal garnet-related Li-ion conductors.

4. Conclusion

Polycrystalline specimen of tetragonal $Li_7La_3Hf_2O_{12}$ with the garnet-related type structure has been successfully synthesized by solid state reaction. This compound is a new member of the fast Li-ion conductor having garnet-related type structure. The chemical composition was analytically determined by ICP-OES. The crystal structure was analyzed by the Rietveld method using ND data. The structure analysis identified that tetragonal $Li_7La_3Hf_2O_{12}$ had the garnet-related type structure with a space group of $I4_1/acd$ (no. 142). The lattice constants were $a = 13.106(2)$ Å and $c = 12.630(2)$ Å with a cell ratio of $c/a = 0.9637$. The crystal structure of tetragonal $Li_7La_3Hf_2O_{12}$ had the garnet-type framework structure composed of dodecahedral $La(1)O_8$, $La(2)O_8$, and octahedral HfO_6. Li atoms occupied three types of crystallographic site in the interstices of this framework structure, where Li(1) atom was located at the tetrahedral 8*a* site, and Li(2) and Li(3) atoms were located at the distorted octahedral 16*f* and 32*g* sites, respectively. These Li sites were filled with the Li atom. The XRD pattern of tetragonal $Li_7La_3Hf_2O_{12}$ was also identified as the structure model determined by the ND analysis. The present tetragonal $Li_7La_3Hf_2O_{12}$ sample exhibited a bulk Li-ion conductivity of $\sigma_b = 9.85 \times 10^{-7}$ S cm^{-1} and grain-boundary Li-ion conductivity of $\sigma_{gb} = 4.45 \times 10^{-7}$ S cm^{-1} at 300 K. The activation energy was estimated to be $E_a = 0.53$ eV in the temperature range of 300–580 K. The Li-ion conductivity of tetragonal $Li_7La_3Hf_2O_{12}$ was slightly lower than that of tetragonal $Li_7La_3Zr_2O_{12}$.

Acknowledgment

This research was supported by Research Fellowships from the Japan Society for the Promotion of Science for Young Scientists (18-1415).

Appendix A. Supplementary material

Supplementary data associated with this article can be found in the online version at 10.1016/j.jssc.2009.10.030.

References

[1] R. Murugan, V. Thangadurai, W. Weppner, Angew. Chem. Int. Ed. 46 (2007) 7778.
[2] A. Kaeriyama, H. Munakata, K. Kajihara, K. Kanamura, Y. Sato, T. Yoshida, ECS Trans. 16 (24) (2009) 175.
[3] V. Thangadurai, W. Weppner, J. Am. Ceram. Soc. 88 (2) (2005) 411.
[4] M.P. O'Callaghan, A.S. Powell, J.J. Titman, G.Z. Chen, E.J. Cussen, Chem. Mater. 20 (2008) 2360.
[5] E.J. Cussen, T.W.S. Yip, J. Solid State Chem. 180 (2007) 1832.
[6] R. Murugan, W. Weppner, P. Schmid-Beurmann, V. Thangadurai, Mater. Sci. Eng. B 143 (2007) 14.
[7] V. Thangadurai, H. Kaack, W.J.F. Weppner, J. Am. Ceram. Soc. 86 (3) (2003) 437.
[8] R. Murugan, V. Thangadurai, W. Weppner, J. Electrochem. Soc. 155 (1) (2008) A90.
[9] V. Thangadurai, J. Schwenzel, W. Weppner, Ionics 11 (2005) 11.
[10] V. Thangadurai, W. Weppner, Adv. Funct. Mater. 15 (1) (2005) 107.
[11] V. Thangadurai, W. Weppner, J. Power Sources 142 (2005) 339.
[12] R. Murugan, V. Thangadurai, W. Weppner, Ionics 13 (2007) 195.
[13] R. Murugan, V. Thangadurai, W. Weppner, Appl. Phys. A 91 (2008) 615.
[14] J. Awaka, N. Kijima, Y. Takahashi, H. Hayakawa, J. Akimoto, Solid State Ionics 180 (2009) 602.
[15] E.J. Cussen, Chem. Commun. (2006) 412.
[16] M.P. O'Callaghan, E.J. Cussen, Chem. Commun. (2007) 2048.
[17] I.P. Roof, M.D. Smith, E.J. Cussen, H.-C. zur Loye, J. Solid State Chem. 182 (2009) 295.
[18] J. Percival, P.R. Slater, Solid State Commun. 142 (2007) 355.
[19] J. Awaka, N. Kijima, H. Hayakawa, J. Akimoto, J. Solid State Chem. 182 (2009) 2046.
[20] J. Percival, E. Kendrick, R.I. Smith, P.R. Slater, Dalton Trans. (2009) 5177.
[21] K.-H. Hellwege (Ed.), Magnetic and Other Properties of Oxides and Related Compounds. Part b: Landolt–Börnstein, New Series, Group III: Crystal and Solid State Physics, vol. 4, Springer, Berlin, Heidelberg, New York, 1970, p. 1 (and references therein).
[22] J. Awaka, R. Katagi, H. Sasaki, R. Endoh, N. Matsumoto, S. Ebisu, S. Nagata, J. Phys. Chem. Solids 62 (2001) 743.
[23] J. Awaka, T. Kurimoto, S. Nagata, J. Phys. Chem. Solids 64 (2003) 2403.
[24] J. Awaka, R. Endoh, S. Nagata, J. Phys. Chem. Solids 64 (2003) 2403.
[25] J. Awaka, M. Ito, T. Suzuki, S. Nagata, J. Phys. Chem. Solids 66 (2005) 851.
[26] J. Awaka, N. Kijima, M. Uemura, Y. Kawashima, S. Nagata, J. Phys. Chem. Solids 66 (2005) 103.
[27] J. Awaka, N. Kijima, J. Akimoto, S. Nagata, J. Phys. Chem. Solids 69 (2008) 1740.
[28] K. Ohoyama, T. Kanouchi, K. Nemoto, M. Ohashi, T. Kajitani, Y. Yamaguchi, Jpn. J. Appl. Phys. 37 (1998) 3319.
[29] F. Izumi, T. Ikeda, Mater. Sci. Forum 321–324 (2000) 198.
[30] K. Momma, F. Izumi, J. Appl. Crystallogr. 41 (2008) 653.
[31] B.D. Cullity, Elements of X-Ray Diffraction, second ed., Addison-Wesley Pub. Co., USA, 1978.
[32] M.U. Cohen, Rev. Sci. Instrum. 6 (1935) 68.
[33] M.U. Cohen, Rev. Sci. Instrum. 7 (1936) 155.
[34] R.A. Young, in: R.A. Young (Ed.), The Rietveld Method, Oxford University Press, Oxford, 1995 (Chapter 1).
[35] R.D. Shannon, Acta Crystallogr. A 32 (1976) 751.
[36] J.V. Smith, B. Mason, Science 168 (1970) 832.
[37] A. Nakatsuka, A. Yoshiasa, T. Yamanaka, O. Ohtaka, T. Katsura, E. Ito, Am. Mineral. 84 (1999) 1135.
[38] K. Fujino, H. Momoi, H. Sawamoto, M. Kumazawa, Am. Mineral. 71 (1986) 781.
[39] D.M. Hatch, S. Ghose, Am. Mineral. 74 (1989) 1221.